Numerical study of the influence of picosecond laser spot size on laser ablation of metal for high laser fluence cases

Yiming Zhang [a,b*], Beat Neuenschwander [a], Valerio Romano [a,b]

[a] Bern University of Applied Science, Institute of Applied Laser, Photonics and Surface Technologies, Pestalozzistrasse 20, 3400 Burgdorf, Switzerland
[b] Institute of Applied physics, University of Bern, Sidlerstrasse 5, 3012 Bern, Switzerland

ABSTRACT

Previously the influence of picosecond laser spot size on ablation depth and threshold fluence on copper has been experimentally investigated. In order to have a comprehensive understanding of the corresponding mechanisms for high laser fluence cases, in which the laser fluence is several folds larger than the optimal ablation fluence, an axisymmetric 2D model, combining modified Two Temperature Model (TTM) and hydrodynamics, was developed. Since the dense vapor and plasma shielding effects have a significant impact on the absorbed energy of incident laser on the material surface, especially for the situation where the laser fluence is higher than vaporization threshold, several assumptions were made. It was roughly supposed that when the lattice temperature reaches $0.9T_c$ (T_c denotes the critical temperature of copper) dense vapor forms above the surface of the material due to the homogenous nucleation within the superheated melted layer, and once the surface temperature exceeds T_c stronger absorption of incident laser by plasma starts to play a crucial role. As the optical thickness of both dense vapor and plasma were supposed to be constants, correspondingly, the transmittance of both layers were approximately evaluated. Furthermore, as generally supposed in the literature, considerable energy loss caused by homogenous nucleation was also taken into account once the surface temperature of the lattice increased to $0.9T_c$, and the melted material was treated as weakly compressible laminar flow with low Mach number ($Ma<0.3$). The numerical results indicate that the kinetic energy of the evaporated material increases when the laser spot size decreases, which could be a possible mechanism of the deeper ablation depth per pulse observed in the experiments with smaller laser spot sizes. Due to the occurrence of phase explosion, the surface temperature keeps constantly around $0.9T_c$, and the intensive evaporation could remain the temperature at T_c until the establishment of equilibrium of both subsystems. Finally, the calculated evaporated mass has the same order of magnitude as the corresponding experimental data.

Keywords: picosecond pulsed laser, laser spot size, thermal-hydrodynamic model, ablation efficiency

1. INTRODUCTION

Characterized by the outstanding precision and high throughputs, ultrashort pulsed laser has been widely used in various of applications, such as microprocessing, 3D printing and thin film deposition. Especially in the field of laser microprocessing, accompanying with the development of new types of laser, the limitation of these features is always challenged by carrying out updated strategies, saying laser ablation with burst mode [1-3], synchronization of laser and ultrafast scanning techniques [4-5] and beam shaping [6-7]. The influence of beam spot size, as one of the adaptable laser parameters, on laser ablation efficiency is, however, rarely reported. As early as in 1987, M. Eyett and D. Bäuerle [8] found out that irradiated by excimer laser, the ablation rate of $LiNbO_3$ (µm/pulse) increased by a factor of 3 for smaller spot size ($\phi = 24\mu m$) compared with larger ones ($\phi > 80\mu m$), where the ablation rate was saturated. The spot size effect on the propagation of laser induced plasma was investigated in [9], finding out that sharpening of plume depends strongly on spot size, as well as the plume expansion. Recently the ablation rate (µm/pulse) induced by ArF excimer laser on Al was found to be strongly dependent on laser spot size [10]. The extended defect model described in [11] was used to interpret such dependency upon fs laser ablation threshold on silicon and stainless steel. In our previous work [12]

---

[*] yiming.zhang@bfh.ch; phone +41 (0)34 426 43 59; alps.ti.bfh.ch

Laser Applications in Microelectronic and Optoelectronic Manufacturing (LAMOM) XXII, edited by
Beat Neuenschwander, Costas P. Grigoropoulos, Tetsuya Makimura, Gediminas Račiukaitis, Proc. of SPIE
Vol. 10091, 100910S · © 2017 SPIE · CCC code: 0277-786X/17/$18 · doi: 10.1117/12.2253629

the experiment of laser ablation on copper by 10ps laser with different spot sizes and corresponding results were presented. In this work a 2D axisymmetric model dealing with thermal ablation is developed to systematically investigate the spot size effect on ultrashort pulsed laser ablation with metal and corresponding numerical results are compared with the experimental ones.

2. SIMULATION

On the basis of Finite Element Method (FEM) the 2D model combined Two Temperature Model (TTM) with Naiver-Stocks equations in hydrodynamics is established. The melted layer is regarded as weakly compressible fluid with low Mach number (Ma<0.3). The governing equations and corresponding boundary conditions and initial values are as following

2.1 Governing equations

$$C_e(T_e)\frac{\partial T_e}{\partial t}+\nabla\cdot(-\kappa_e(T_e)\nabla T_e)=-G(T_e)(T_e-T_l)+S(r,z,t) \tag{1}$$

$$C_l\frac{\partial T_l}{\partial t}+\nabla\cdot(-\kappa_l\nabla T_l)+C_l\vec{v}(r,z)\cdot\nabla T_l=G(T_e)(T_e-T_l)-Q \tag{2}$$

$$\begin{aligned}&\rho\frac{\partial\vec{v}(r,z)}{\partial t}+\rho(\vec{v}(r,z)\cdot\nabla)\vec{v}(r,z)=\\&\nabla\cdot[-P\vec{I}+\mu_l(\nabla\vec{v}(r,z)+(\vec{v}(r,z))^T)-\frac{2}{3}\mu_l(\nabla\cdot\vec{v}(r,z))\vec{I}]+\vec{F}_{vol}\end{aligned} \tag{3}$$

$$\frac{\partial\rho}{\partial t}+\nabla\cdot(\rho\vec{v}(r,z))=0 \tag{4}$$

Where $C_e(T_e)$ and C_l are electron-temperature dependent electronic heat capacity and lattice heat capacity, respectively, $\kappa_e(T_e)$ is electron-temperature dependent electronic thermal conductivity, κ_l is lattice thermal conductivity, $G(T_e)$ is electron-temperature dependent electron-phonon coupling coefficient. Because of the higher laser fluence applied in the model the thermal properties mentioned above holds in the situation where the lattice temperature higher than the critical temperature. The thermal source term of Gaussian laser beam, spatially and temporally, is given $S(r,z,t)=\alpha^{-1}(1-R)\frac{F_{peak}}{\tau_p}\exp(\frac{r^2}{\omega_0^2})\exp(-\alpha^{-1}z)\sqrt{4\ln 2/\pi}\exp(4\ln 2(\frac{t-2\tau_p}{\tau_p})^2)$, where the absorption coefficient α and reflectivity R, based on critical model of optical property [13], are the function of temperature of both subsystems. F_{peak} is the peak fluence of pulsed laser. τ_p and ω_0 are pulse duration and beam radius, respectively. μ_l is the dynamic viscosity of copper, $\vec{I}$ is the unit matrix and $\vec{F}_{vol}$ is the body force, $\vec{F}_{vol}=\frac{(1-\mathrm{B})^2}{\mathrm{B}^3+\zeta}\mathrm{A}_{\mathrm{mush}}\vec{v}(r,z)+\vec{g}(\rho-\rho_\infty)$, which consists of momentum sinking on the solid-liquid interface and buoyancy induced by the change of density. In this expression, B is the liquid volume fraction, which reads as

$$\mathrm{B}=\begin{cases}1 & \mathrm{T}>(\mathrm{T_m}+\delta\mathrm{T})\\ \frac{(\mathrm{T}-\mathrm{T_m}+\delta\mathrm{T})}{2\delta\mathrm{T}}, & (\mathrm{T_m}-\delta\mathrm{T})\le\mathrm{T}\le(\mathrm{T_m}+\delta\mathrm{T})\\ 0 & \mathrm{T}<(\mathrm{T_m}-\delta\mathrm{T})\end{cases}$$

. ζ is a small number using to prevent division by zero. $\mathrm{A_{mush}}$ is the mushy zone constant, measuring the amplitude of the damping. Specifically, the higher this value is, the steeper the transition of the velocity of the melted material to zero as it solidifies could be. ρ_∞ is the undisturbed constant density, which equals to the solid density of copper in the model.

It should be noted that by considering the dense vapor and plasma shielding effect induced by laser beam with high power density, the heat source term in equation (1) should be modified. When the heterogeneous evaporation takes place the vapor layer above interphase is still transparent to the incident beam, while as the evaporation becomes more intensive the vapor layer begins to absorb part of laser energy, turning to be semitransparent. Generally speaking, once the temperature of material reaches critical temperature the overheated vapor might start to ironize and forms the plasma, attributed to the further absorption of laser energy. Although the aerodynamics of dense vapor and plasma is complicated, because of the self-adjustment mechanism, where the absorption of plasma increases less energy reaches the surface of material weakening the evaporation, and in turn enhancing the energy coupling on material surface, the optical thickness in both layers can be approximately regarded as constant. Therefore the deduced absorption coefficients of dense vapor and plasma layers are $e^{-0.28}$ and e^{-1}, respectively [14].

In addition, it is generally accepted that phase explosion occurs when the temperature of ablated material reaches $0.9T_c$, which implies the super-heated material in such metastable state might follow an adiabat below critical point. Specifically, based on the theory of metastable liquid [15], the superheated liquid by rapid heating might undergo the shifting from binodal into metastable states, even close to spinodal depending on the degree of heating of the material. Then the liquid layer seeks for equilibrium following the way of returning the binodal through phase explosion, as demonstrated in Figure 1. The homogenous nucleation rate during this process determines the lifetime of the metastable state. In the model it is supposed that when the lattice temperature reaches $0.9T_c$ after the termination of pulsed laser phase explosion takes place, otherwise this effect could be suppressed since on the one hand the time could be too short for the generated nucleation to reach the critical size, and on the other hand the shielding effect induced by dense vapor and plasma could influence the pressure above the evaporated surface. Predicted by this model, for the case where the peak laser fluence is larger than 6 J/cm^2 holds this criterion. The homogenous nucleation rate per unit volume according to classical nucleation theory is referred to calculate the energy loss caused by phase explosion [16].

$J = N_1(\frac{3\sigma_{Cu}}{\pi M})^{1/2} \exp(\frac{-4\pi r_c^2 \sigma_{Cu}}{3k_B T_l})$, where N_1 is the number of the liquid molecule per unit volume, σ_{Cu} is the surface tension, M is the molecular weight of melted copper, k_B is Boltzmann constant. r_c denotes the critical radius of bubble, given by

$r_c = \frac{2\sigma_{Cu}}{P_s \exp(\frac{-2\sigma_{Cu}}{\rho R_g T_l})}$, where R_g is the ideal gas constant. Generally speaking, with an external action, e.g. radiation, homogenous nucleation could occur instantaneously when the temperature exceeds approximately $0.9T_c$. Therefore, in the process of laser ablation, the melted copper will intensively explode in the form of liquid droplets and massive vapors. Furthermore, considerable energy could be carried away due to the dramatically removed material. Such energy loss is applied as volumetric heat source in the region where the temperature exceeds $0.9T_c$ in the model, given by $Q = -\frac{1}{2}mv^2 J$, here it is assumed that the average kinetic energy of the removed material to some extent equals to the potential energy of mutual attraction of the molecules, which is based on the definition of critical point.

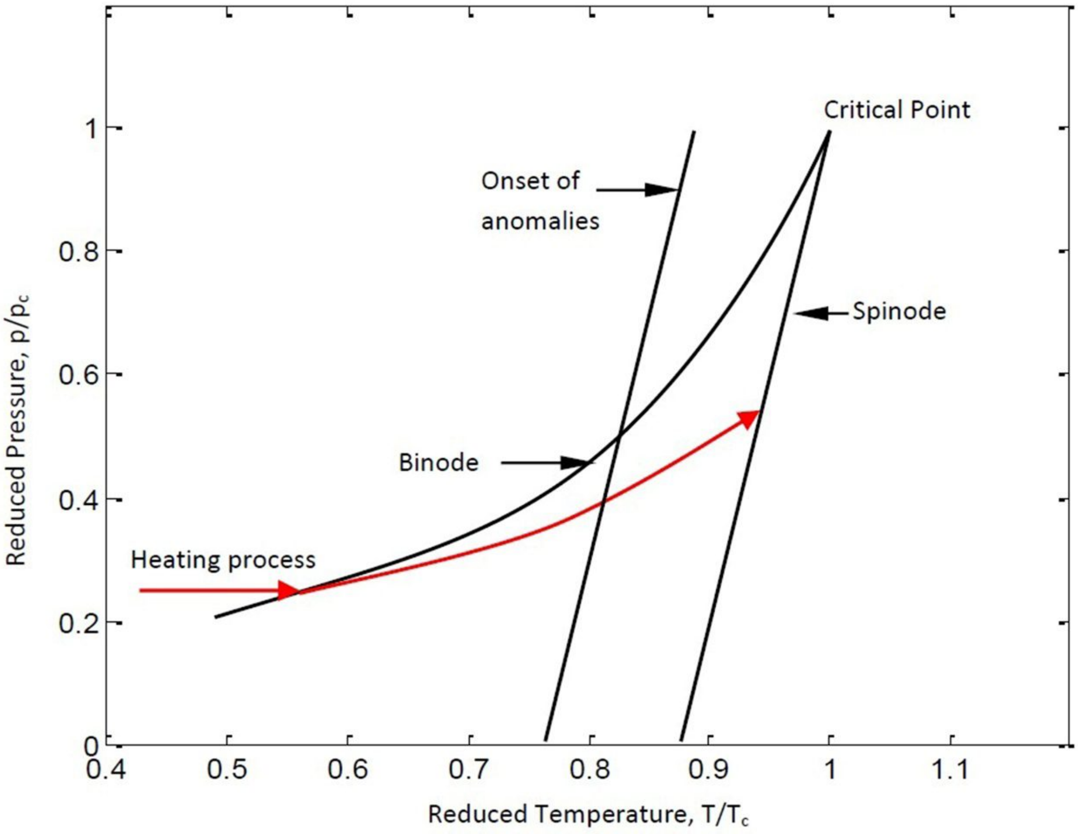

Figure 1 The concept of explosive boiling, including bimodal and spinodal, and the red curve shows a typical heat cycle.

2.2 Boundary conditions and initial values

For the electron subsystem, the energy loss caused by thermionic emission is considered. $\kappa_e(T_e)\nabla T_e = -(E_f + \phi)\dot{N}$, where $E_f + \phi$ is the potential barrier for an electron to be removed from the metal equaling to the sum of Fermi energy and work function of copper, the kinetic energy of the escaping electron is neglected. $\dot{N} = \frac{A_0}{e} T_e^2 \exp(-\frac{e\phi}{k_B T_e})$ is the electron emission rate derived from Richardson-Dushman equation. For the lattice subsystem the energy loss attributed to the evaporation and surface thermal emission are taken into account. $\kappa_l \nabla T_l = -L_v v_e \rho_L - \sigma\varepsilon(T_l^4 - T_0^4)$, where L_v is the latent heat of vaporization of copper, v_e is the recession speed of the vaporization front obtained from the mass flux of vapor evaporated from a liquid surface described by the Hertz-Knudsen formula when the surface temperature is below T_c and by solving aerodynamic equations [14] when the surface temperature exceeds T_c , ρ_L is the liquid density of copper, and ε is the surface emissivity of copper. Both Marangoni effect and recoil pressure are applied as the boundary conditions of Navier-Stocks equations.

$[-P\vec{I} + \mu_l(\nabla\vec{v}(r,z) + (\vec{v}(r,z))^T) - \frac{2}{3}\mu_l(\nabla\cdot\vec{v}(r,z))\vec{I}]\vec{n} = -\mathrm{P}_{\mathrm{recoil}}\vec{i} + \frac{\partial\sigma_{\mathrm{Cu}}}{\partial\mathrm{T}}\frac{\partial\mathrm{T}}{\partial x}\vec{j}$, where the normal component, $\vec{i}$, is recoil pressure P_{recoil} , which is due to the metallic vapor after the surface temperature exceeds the boiling point, in the opposite direction. The recoil pressure of the evaporating vapor P_{recoil} is approximate $0.54P_{sat}$. The saturated pressure of the vapor at the evaporation surface is obtained from the Clausius-Clayperon relation. $P_{sat} = P_{amb}\exp(\frac{L_v M}{k_B T}(\frac{T_l}{T_b}-1))$, where P_{amb} is the ambient pressure, which equals to 1 atm. The tangential component, $\vec{j}$, is Marangoni effect caused by the gradient of surface tension along the radial direction.

Both the initial temperatures of electron and lattice subsystems are room temperature $T_0 = 300K$. The initial velocity and pressure are $\vec{u} = 0$ and $P = 0$, respectively.

2.3 Physical properties

As the laser fluence applied in the model is relatively higher than moderate one, the generic forms of the variables, which depend on temperature and hold in extreme situation, are employed in the model.

$$C_e(T_e) = \begin{cases} C_{e0}T_e & T_e < T_F / \pi^2 \\ 2C_{e0}T_e/3 + C'_e/3 & T_F/\pi^2 \le T_e < 3T_F/\pi^2 \\ Nk_B + C'_e/3 & 3T_F/\pi^2 \le T_e < T_F \\ 3Nk_B/2 & T_e \ge T_F \end{cases},$$

Where $C_{e0} = \frac{1}{2}\frac{\pi^2 k_B N}{T_F}$, $C'_e = C_{e0}T_F/\pi^2 + \frac{3Nk_B/2 - C_{e0}T_F/\pi^2}{T_F - T_F/\pi^2}(T_e - T_F/\pi^2)$

The lattice thermal conductivity is taken as 1% of the thermal conductivity of bulk metal, $\kappa_l = 0.01\kappa_0$, since the mechanism of heat conduction in metals is dominated by electrons [17].

In the higher laser fluence case the electronic thermal conductivity reads [18] $\kappa_e = C\theta_e \frac{(\theta_e^2 + 0.164)^{5/4}(\theta_e^2 + 0.44)}{(\theta_e^2 + 0.092)^{1/2}(\theta_e^2 + b\theta_l)}$, where $\theta_e = \frac{T_e}{T_F}$, $\theta_l = \frac{T_l}{T_F}$

This is valid up to the Fermi temperature, T_F.

The electron-temperature dependent electron-lattice coupling coefficient are obtained by fitting the computed data in [19] based on the assumption that the square of the absolute electron-phonon scattering matrix elements, when summed over the scattering angles, is independent of the electron state.

$$G(T_e) = \begin{cases} 0.56\times 10^7, T_e < 2750K \\ 1.341\times 10^7 - 1.407\times 10^{14}T_e + 5.988\times 10^{10}T_e^2 - 7.93\times 10^6 T_e^3 \\ +555.2T_e^4 - 0.023272T_e^5 + 6.041\times 10^{-7}T_e^6 - 9.529\times 10^{-12}T_e^7 \\ +8.377\times 10^{-17}T_e^8 - 3.15\times 10^{-22}T_e^9 \end{cases}, 2750K \le Te \le 5\times 10^4 K$$

The lattice temperature dependent dynamic viscosity [20] and surface tension coefficient [21] are $10^{-3}\times 10^{(-0.422+1393.4/T_l)}$ and $1.497 - 1.74\times 10^{-4}T_l$, respectively. Other physical properties applied in the model are listed in Table 2.

Table 2. The physical properties of copper [18, 22-25]

Nomenclature and Value		
A_0	Richardson's constant	$1.2\times10^6 A/(m^2K^2)$
b	Coefficient of electron thermal conductivity	0.139
C	Coefficient of electron thermal conductivity	$377 Wm^{-1}K^{-1}$
C_l	Lattice specific heat capacity	$3.5\times10^6(J/m^3K)$
e	Charge of electron	$1.6022\times10^{-19}C$
E_f	Fermi energy	$7eV$
E_{Tiso}	Isotropic tangent module	$1.25\times10^8 Pa$
k_B	Boltzmann constant	$1.38\times10^{-23} m^2kgs^{-2}K^{-1}$
L_m	Latent heat of fusion	$205000(J/kg)$
L_v	latent heat of vaporization	4796000(J/kg)
M	Molecular mass of copper	$1.0552\times10^{-25}kg$
N	Number density of free electron	$8.41\times10^{28}(1/m^3)$
T_0	Initial value of temperature	$300K$
T_F	Fermi temperature	81200K
T_c	Critical point	7696K
Greek symbols		
ρ_s	Solid density of copper	$8.9 g/cm^3$
ρ_L	Liquid density of copper	$8.02 g/cm^3$
ρ_g	Gas density of copper	$6.792 g/cm^3$
ρ_c	Copper density at critical point	$1.04 g/cm^3$
κ_0	Coefficient of lattice thermal conductivity	$400(Jm^{-1}s^{-1}K^{-1})$
ϕ	Work function	$4.6eV$

Subscripts			
e	Electron	v	Vapor
l	Lattice	L	Liquid
g	Gas	c	Critical
s	Solid		

3. RESULTS AND DISCUSSION

Various laser peak fluences ranging from 2J/cm^2 to 10J/cm^2 with three different spot sizes, namely 15.5µm, 31.5µm and 49.6µm, are applied in the model. The temperature profiles of both subsystems are shown in Figure 2.

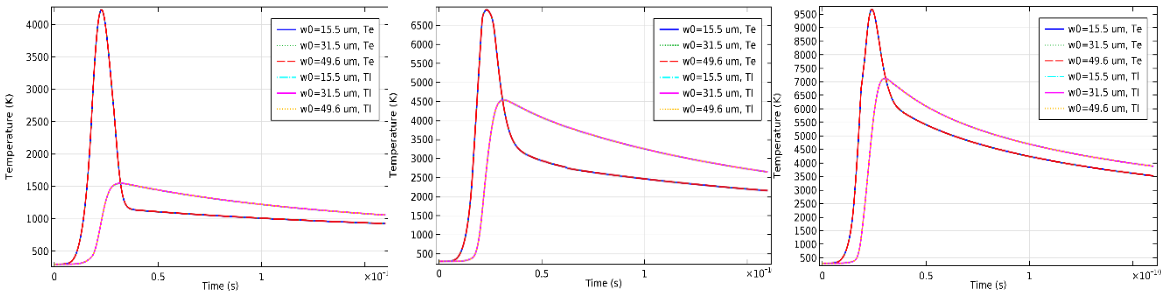

(a) (b) (c)

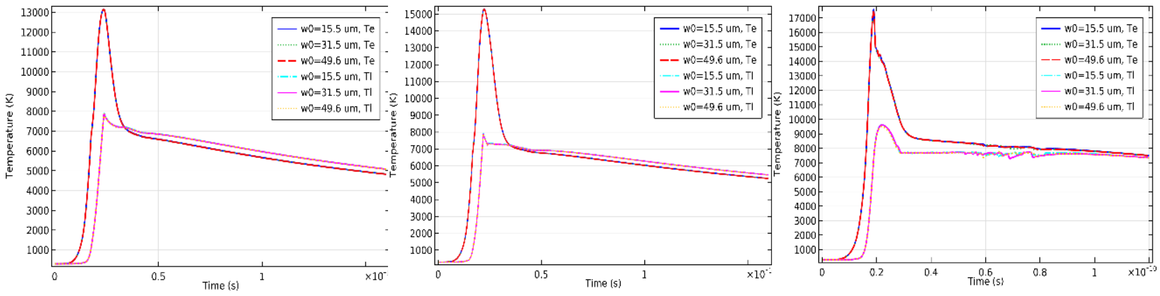

(d) (e) (f)

Figure 2 The temperature profiles of electron and lattice subsystems at the center of material, (a) 2J/cm^2, (b) 3J/cm^2, (c) 4J/cm^2, (d) 5J/cm^2, (e) 6J/cm^2, (f) 7J/cm^2

The temperature profiles of both subsystems are almost the same for all the spot sizes in each laser ablation case. As the increasing of laser peak fluence the material undergoes melting (Fig.2 (a)), evaporation (Fig.2 (b), (c)) and intensive boiling (Fig.2 (d), (e) and (f)). Due to phase explosion (Fig.2 (d), (e)) the lattice temperature drops down rapidly when it reaches critical temperature and enters the saturation stage before both subsystems further reach equilibrium. The higher the fluence is, the longer time the saturated stage can keep, which is attributed to the thermal dynamic behaviors of energy coupling within electron-lattice systems and lattice energy loss induced by homogenous nucleation. As the lattice temperature reaches the critical temperature before the termination of pulsed laser in the even higher laser peak fluence case (Fig.2 (f)), the energy loss is dominated by the extremely intensive evaporation. When the lattice temperature drops to critical temperature, the material remains in the saturated state because of equilibrium of thermal dynamics until the two subsystems reach equilibrium. Such process is more significant than the similar phenomenon caused by homogenous nucleation. Under such extremely heated conditions, considerable amount of material could be intensively removed in the forms of vapor and small droplets from the surface. The profiles of kinetic energy density of the removed material for all spot sizes are shown in Figure 3.

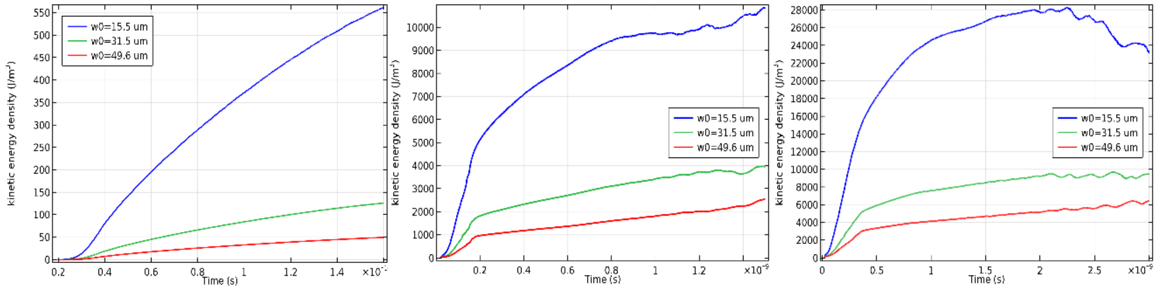

(a) (b) (c)

Figure 3 The kinetic energy density of the removed material as the function of time, (a) 6J/cm^2, (b) 7J/cm^2, (c) 10J/cm^2

It is found that the kinetic energy density of removed material in all the smallest spot size cases is significantly higher than other two cases. Therefore, this might be a possible explanation for the spot size effect on ablation rate in terms of depth per pulse. Specifically, since the removed material induced by irradiation with smaller spot size contains more kinetic energy, higher average velocity can be achieved with the assumption of identical average mass of the removed material in unit volume. Furthermore, along the direction of depth, more material can be removed in unit time, leading to a deeper ablation depth. The profiles of the mass of the removed material in all spot size cases are presented in Figure 4.

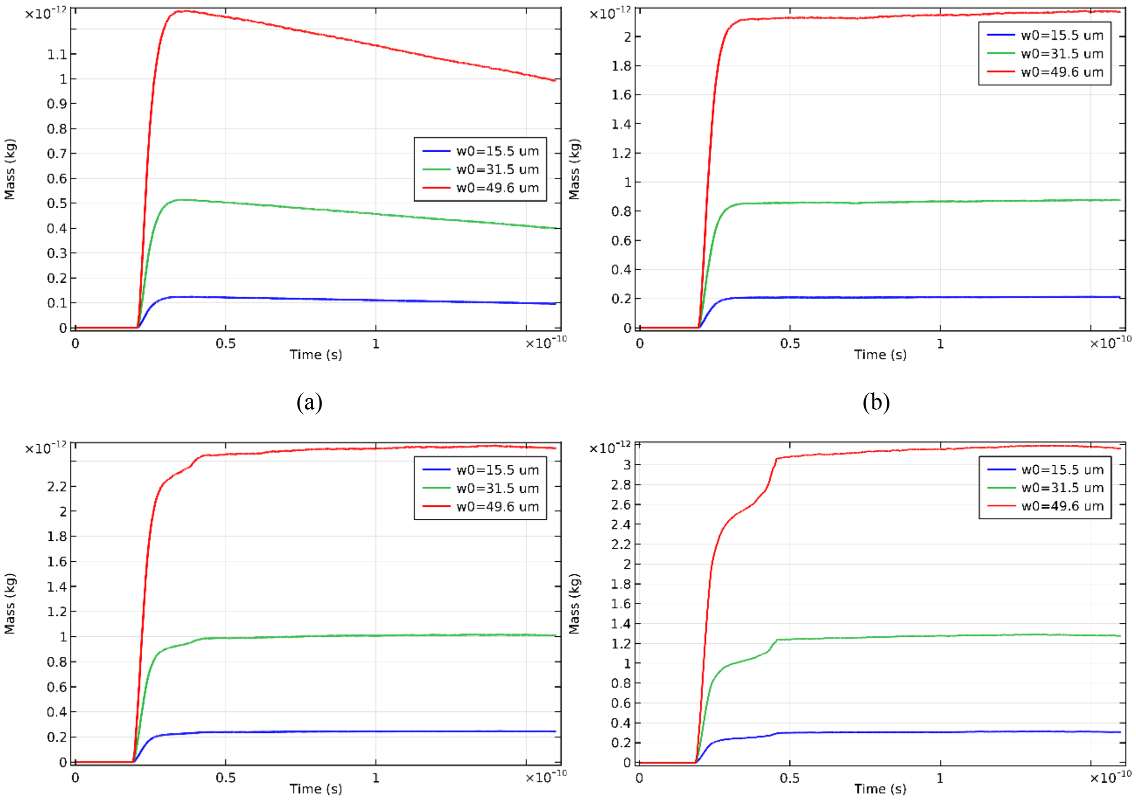

(a) (b) (c) (d)

Figure 4 The profiles of mass of removed material, (a) 3J/cm^2, (b) 4J/cm^2, (c) 5J/cm^2, (d) 6J/cm^2

As the increase of laser fluence, the time when the ablation takes place becomes earlier due to the increase of temperature raising rate. They are approximate 20.6ps, 19.4ps, 19.1ps and 18.6ps for 3J/cm^2, 4J/cm^2, 5J/cm^2 and 6J/cm^2, respectively. Since the maximum lattice temperature in the cases of fluence below 4J/cm^2 is lower than the critical temperature, seeing Figure 2 (b) and (c), the mass of removed material only follows the normal path, along which the mass increases due to normal boiling and decreases because of cooling of material. For the higher fluences, seeing Figure 2 (d) and (e), there is an abruptly rapid increase of mass attributed to the initiation of phase explosion, since the lattice temperature of corresponding time just satisfies the criterion of triggering the phase explosion. The correspondingly experimental results of the ablated mass as the function of laser peak fluence for the three different spot sizes are demonstrated in Figure 5, comparing with the simulation.

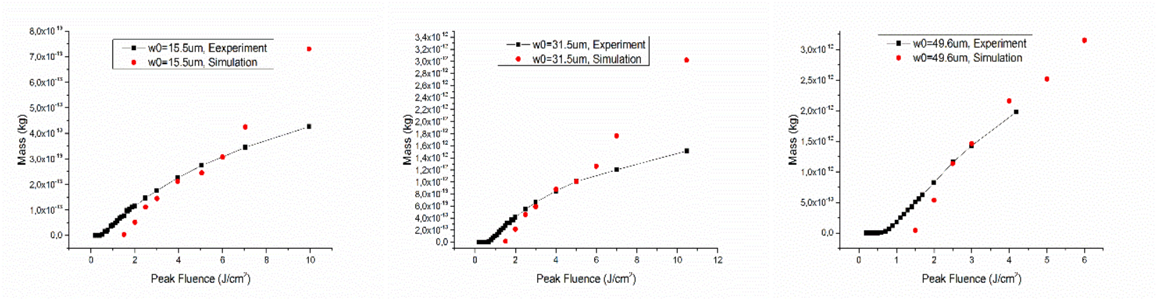

(a) (b) (c)

Figure 5 Comparison of experimental and simulated results of mass of removed material, (a)15.5μm, (b) 31.5μm and (c) 49.5μm

Both of the data agree well with each other except the ones for the peak fluences lower than 2J/cm^2 and higher than 6J/cm^2. On one hand, as shown in Figure 2 (a), the lattice temperature of material is just slightly above melting point and only limited area adjacent to the center is melted. Therefore, under such circumstance major part of the removed material is still induced by spallation with the help of thermal stress. On the other hand, due to the extremely intensive evaporation above the superheated surface, significant amount of evaporated material could return to the surface under the force of recoil pressure after the plasma layer, which is not taken into account in the model. The simulated results of total removed mass and the removed mass by evaporation and phase explosion for all three spot sizes cases are compared in Figure 6.

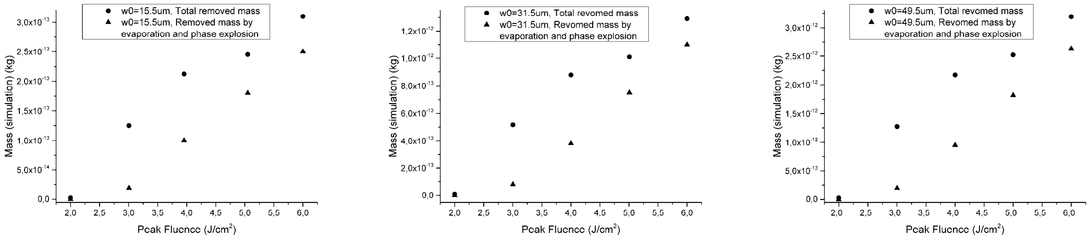

(a) (b) (c)

Figure 6 Comparison of total removed mass and removed mass by evaporation and phase explosion for spot size of (a) 15.5μm, (b) 31.5μm and (c) 49.5μm

As indicated for all different spot size cases the deviation between the total removed mass and the removed mass by evaporation and phase explosion becomes smaller as the peak fluence increase from 3J/cm^2 to 6J/cm^2, illustrating the evaporation and phase explosion carry more and more weight in the process of laser ablation and become the dominated mechanism of material removal. Further comparison of experimental and simulated results is carried out in terms of removal rate with the unit of μm^3/μJ, shown in Figure 7.

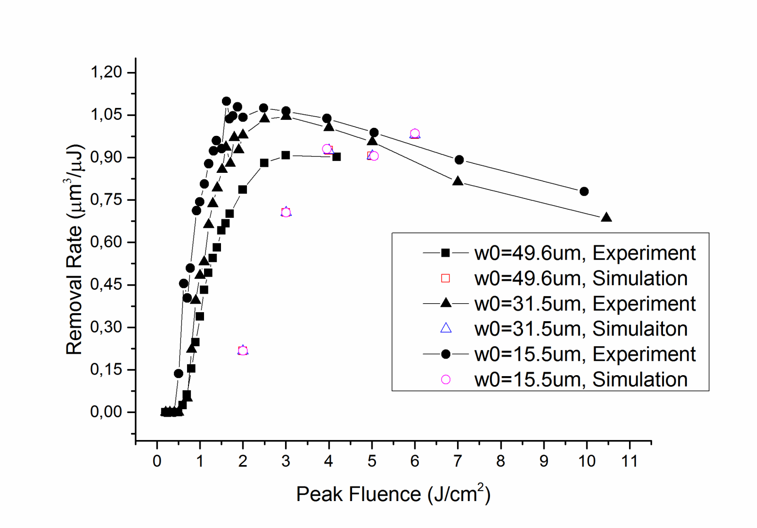

Figure 7 Comparison of removal rate of different laser spot sizes

The simulated results of removal rate for the peak fluences between 2/cm^2 to 6J/cm^2 match well with the experimental ones. In addition, the dependence of removal rate on spot size no longer exists when it is evaluated with unit ablated volume by unit energy (μm^3/μJ). Similar to experiment results there is an optimal peak fluence for laser ablation regardless of spot size.

4. CONCLUSION

The spot size effects on laser ablation on copper with high peak fluence 10 ps pulsed laser have been numerically studied and compared with corresponding experimental results. By establishing the 2D model, based on Two Temperature Model (TTM) and hydrodynamics, the dependence of kinetic energy density of removed material on spot size is found. It demonstrates that in the center of ablated area the removed material carries more kinetic energy when the target is irradiated with smaller spot size. This could be a possible mechanism of the higher ablation rate obtained by beam with smaller spot size. Additionally, for the cases of peak fluence between $2J/cm^2$ and $6J/cm^2$ the good agreement between experimental and simulated results on the mass of removed material for all spot size indicates the validity of the models. The overestimated results of mass of removed material for extremely high cases, on one hand, demonstrate the limitation of current model, and on the other hand, imply the probably redeposition of evaporated material influenced by the recoil pressure. By comparing the mass of removed material in different ways, the dynamic behaviors of ablation are clear. Spallation is the major mechanism of mass removal for the laser fluence below and slightly above melting threshold, while for the higher fluence evaporation and even phase explosion become the dominated mechanisms instead of removal of melting material. Finally, the dependence of ablation behavior on spot size vanishes when it turns to comparison of removal rate in terms of ablated volume per unit energy, but the results of both experiment and simulation reflect the optimal peak fluence, which could be helpful for finding the strategy to increase the ablation efficiency with ultrashort pulsed laser.

5. ACKNOWLEGMENTS

The author would like to thank the Know-how and Technology Transfer department of the Bern University of Applied Science for its financial support.

REFERENCES

[1] B. Neuenschwander, Th. Kramer, B. Lauer, B. Jaeggi, “Burst mode with ps- and fs-pulses: Influence on the removal rate, surface quality, and heat accumulation”, *Proc. SPIE* 9350, Laser Applications in Microelectronic and Optoelectronic Manufacturing (LAMOM) XX, 93500U (2015).

[2] Franziska Bauer, Andreas Michalowski, Thomas Kiedrowski, and Stefan Nolte, “Heat accumulation in ultra-short pulsed scanning laser ablation of metals”, Optics Express, 23 (2), 1035 (2015).

[3] N. Hänel, M. Stolze, T. Herrmann, and J. A. Lhuillier, “Fundamental investigations of ps-laser burst-mode on common metals for an enhanced ablation process”, *Proc. SPIE* 9351, Laser-based Micro- and Nanoprocessing IX, 93510E (2015).

[4] Stephan Bruening, Guido Hennig, Stephan Eifel, Arnold Gillner, “Ultrafast Scan Techniques for 3D-μm Structuring of Metal Surfaces with high repetitive ps-laser pulses”, Physics Procedia. 12, 105-115 (2011).

[5] M Zimmermann, B Jaeggi, and B. Neuenschwander, “Improvements in ultra-high precision surface structuring using synchronized galvo or polygon scanner with a laser system in MOPA arrangement”, *Proc. SPIE* 9350, Laser Applications in Microelectronic and Optoelectronic Manufacturing (LAMOM) XX, 935016 (2015).

[6] R. Stoian, J. P. Colombier, C. Mauclair, G Cheng, M. K. Bhuyan, P. K. Velpula, P. Srisungsitthisunti, “Spatial and temporal laser pulse design formaterial processing on ultrafast scales”, Appl. Phys. A. 114, 119 (2014).

[7] Martin Kraus, Marwan Abdou Ahmed, Andreas Michalowski, Andreas Voss, Rudolf Weber, and Thomas Graf, “Microdrilling in steel using ultrashort pulsed laser beams with radial and azimuthal polarization”, Optics Express. 18(21), 22305 (2010).

[8] M.Eyett and D. Bäuerle, “Influence of the beam spot size on ablation rates in pulsed□laser processing”, Appl. Phys. Lett. 51, 2054 (1987).

[9] S. S. Harilal, “Influence of spot size on propagation dynamics of laser-produced tin plasma”, J. Appl. Phys. 102, 123306 (2007).

[10] M E Shaheen, J E Gagnon and B J Fryer, “Excimer laser ablation of aluminum: influence of spot size on ablation rate”, Laser Phys. 26, 116102 (8pp) (2016).

[11] Aida Naghilou, Oskar Armbruster, Markus Kitzler, Wolfgang Kautek, “Spot size and pulse number dependence of femtosecond laser ablation thresholds of silicon and stainless steel”, Applied Surface Science, Volume 396, Pages 1736–1740 (2017).

[12] Benjamin Lauer, Beat Jaeggi, Yiming Zhang, Beat Neuenschwander, “Measurement of the maximum specific removal rate: unexpected influence of the experimental method and the spot size”, ICALE, Paper M701 (2015).

[13] S.Y. Wang, Y. Ren, C.W. Cheng, J.K. Chen, D.Y. Tzou, “Micromachining of copper by femtosecond laser pulses”, Applied Surface Science. 265, 302-308 (2013).

[14] Afanasiev YuV, Krokhin ON, [Quantum Electrics in Lasers and Masers], part 2, Lebedev Inst. of Physics, Russian Academy, Chapter 2 “Gas-dynamical theory of laser radiation effect”, (1969).

[15] Skripov V.P., [Metastable Liquids], Halsted Press, John Wiley & Sons, New York (1974).

[16] Deepak Marla, Upendra V. Bhandarkar, Suhas S. Joshi, A model of laser ablation with temperature-dependent material properties, vaporization, phase explosion and plasma shielding, Appl. Phys. A. 116 (2014) 273-285.

[17] Y. Zhang and J. K. Chen, “Melting and resolidification of gold film irradiated by nano- to femtosecond lasers”, Appl. Phys. A. 88, 289-297 (2007).

[18] Carsten Schaefer, Herbert M. Urbassek and Leonid V. Zhigilei, “Metal ablation by picosecond laser pulses: A hybrid simulation”, Physical Review B. 66, 115404 (2002).

[19] J. Yang, Y. Zhao and X. Zhu, “Theoretical studies of ultrafast ablation of metal targets dominated by phase explosion”, Appl. Phys. A. 89, 571-578 (2007).

[20] Marc J. Assael, Agni E. Kalyva, Konstantinos D. Antoniadis, R. Michael Banish, Ivan Egry, Jiangtao Wu, Erhard Kaschnitz, and William A. Wakeham, “Reference Data for the Density and Viscosity of Liquid Copper and Liquid Tin”, Journal of Physical and Chemical Reference Data. 39, 033105 (2010).

[21] J. Brillo, I. Egry, “Surface tension of nickel, copper, iron and their binary alloys”, Journal of Materials Science. 40, 2213-2216 (2005).

[22] T. Balasubramani and S. H. Jeong, “Simulation of the thermionic emission during ultrashort pulse laser ablation of metals”, Journal of Physics: Conference Series. 59, 595-599 (2007).

[23] B. H. Christensen, K. Vestentoft, P. Balling, “Short-pulse ablation rates and the two-temperature model”, Applied Surface Science. 253, 6347-6352 (2007).

[24] Yunpeng Ren, C.W. Cheng, J.K. Chen, Yuwen Zhang, D.Y. Tzou, “Thermal ablation of metal films by femtosecond laser bursts”. International Journal of Thermal Sciences. 70, 32-40 (2013).

[25] ASM International, [Atlas of Stress-strain Curve], ASM International, ISBN:087170739X, 9780871707390, (2002).